

Continuum of metastable conical states of monoaxial chiral helimagnets

V. Laliena ¹, S. A. Osorio,^{2,3} D. Bazo ⁴, S. Bustingorry ^{2,3,4} and J. Campo ⁴

¹*Department of Applied Mathematics and Institute of Mathematics and Applications (IUMA), University of Zaragoza C, 50018 Zaragoza, Spain*

²*Instituto de Nanociencia y Nanotecnología (CNEA-CONICET), Nodo Bariloche, S. C. de Bariloche, Río Negro R8402AGP, Argentina*

³*Gerencia de Física, Centro Atómico Bariloche, S. C. de Bariloche, Río Negro R8402AGP, Argentina*

⁴*Aragon Nanoscience and Materials Institute (CSIC-University of Zaragoza) and Condensed Matter Physics Department, University of Zaragoza C, 50009 Zaragoza, Spain*



(Received 21 March 2023; accepted 26 June 2023; published 25 July 2023)

At low temperature and zero applied magnetic field, besides the equilibrium helical state, monoaxial chiral helimagnets have a continuum of helical states differing by the wave number of the modulation. The wave number of these states in units of the equilibrium state wave number is denoted here by p , and accordingly the corresponding states are called the p states. In this work we study in detail the metastability of the p states. The application of an external magnetic field in the direction of the chiral axis has a double effect: On the one hand, it introduces a conical deformation of the p states, and, on the other hand, it destabilizes some of them, shrinking the range of p in which the p states are metastable. If a polarized current is applied along the chiral axis, then the p states reach a steady moving state with a constant velocity proportional to the current intensity. Besides this dynamical effect, the polarized current also induces a conical deformation and reduces the range of stability of the p states. The stability diagram in the plane applied field–applied current intensity has interesting features that, among other things, permits the manipulation of p states by a combination of applied fields and currents. These features can be exploited to devise processes to switch between p states. In particular there are p states with negative p , opening the possibility to helicity switching. The theoretical feasibility of such processes, crucial from the point of view of applications, is shown by micromagnetic simulations. Analogous p states exist in cubic chiral helimagnets and therefore similar effects are expected in those systems.

DOI: [10.1103/PhysRevB.108.024425](https://doi.org/10.1103/PhysRevB.108.024425)

I. INTRODUCTION

Noncollinear magnetic textures such as magnetic helices, domain walls, vortices, or skyrmions are very promising for spintronic applications due to the possibility to control them using different external stimuli, like magnetic fields or polarized electric currents [1–6]. To be useful, these magnetic textures have to be (meta)stable in some part of the relevant parameter space. Noncollinear magnetic textures appear, in particular, as equilibrium states at low temperature in chiral magnets, which are characterized by the presence of a sizable Dzyaloshinskii-Moriya interaction (DMI). The most studied systems of this kind are cubic chiral helimagnets and films with interfacial DMI, which host skyrmions and skyrmion lattices [5–9]. Monoaxial chiral helimagnets, in which the DMI propagates only along a single direction (the chiral axis), have received comparatively less attention. Besides the archetypal CrNb_3S_6 , other known monoaxial chiral helimagnets are MnNb_3S_6 , CrTa_3S_6 , CuB_2O_4 , CuCsCl_3 , $\text{Yb}(\text{Ni}_{1-x}\text{Cu}_x)_3\text{Al}_9$, and $\text{Ba}_2\text{CuGe}_2\text{O}_7$ [10–18].

Not surprisingly, monoaxial chiral helimagnets present also a strong uniaxial magnetic anisotropy (UMA) along the chiral axis, which is of easy-plane type in CrNb_3S_6 . The competition of the exchange interaction, the DMI, the UMA and the applied field determines the equilibrium state at low-enough temperature, where thermal fluctuations are only a minor effect. At zero external field the equilibrium state is

a magnetic helix with wave vector along the chiral axis and wave number determined by the competition of the exchange interaction and the DMI. If a low-enough external field is applied in a direction perpendicular to the chiral axis, then the equilibrium state is a chiral soliton lattice (CSL) [19–22]. If instead the magnetic field is applied in the direction of the chiral axis, then the equilibrium state is a conical state [20,23–27]. These two magnetic textures, the CSL and the conical state, are of different nature: The CSL is solitonic while the conical state is helical. If the field direction is neither perpendicular nor parallel, then the equilibrium state at low magnetic fields is a one-dimensional modulated texture which connects the two limiting cases as the direction of the magnetic field is varied from perpendicular to parallel to the chiral axis [26]. In all cases, for sufficiently large magnetic fields the equilibrium state is the forced ferromagnetic state (FFM), which has a uniform magnetization pointing in the direction of the external field. The different nature of the CSL and the conical states is manifested in the transition to the FFM state: In the former case it is of nucleation type and in the latter of instability type, in de Gennes’s terminology [28]. These two different kinds of phase boundaries are separated by tricritical points in the temperature–applied field phase diagram [27,29]. The phase diagram of monoaxial chiral helimagnets and the nature of the phase boundaries in the temperature–applied magnetic field space, determined experimentally by several groups [24,30–33], agree well with these theoretical predictions.

It was shown in Ref. [34] that, at low temperature, besides the conical equilibrium state a continuum of conical states differing by the wave number and the magnetization component along the chiral axis are local minima of the energy functional of monoaxial chiral helimagnets with external magnetic field applied along the chiral axis. Similar local minima of the energy are present in cubic chiral helimagnets [35]. These conical states, called here p states, include states with helicity opposite to the helicity of the equilibrium state, which, although energetically disfavored by the DMI, remain as metastable states in some range of the applied magnetic field. It is also remarkable that among these continuum of metastable states there are some which are ferromagnetic, with the uniform magnetization pointing to a direction determined by the competition between the UMA and the applied field.

In this work we analyze in detail the properties of these p states of monoaxial chiral helimagnets, clarifying their role as metastable states and studying their behavior under the action of polarized electric currents. One conclusion of this analysis is the possibility of switching between metastable conical states with different wave vectors, including the possibility of helicity switching. This is clearly of great interest for applications. Indeed, it has been argued recently that controlled switching among magnetic states with opposite helicity might be used for memory applications [36].

II. A CONTINUUM OF CONICAL STATES

Consider a monoaxial chiral helimagnet, such as CrNb_3S_6 , with chiral axis along z (we shall use x, y, z as the orthonormal vector triad in space). At low-enough temperature the local magnetization is given by $M_S \mathbf{n}$, where \mathbf{n} is a unit vector field that describes the magnetization direction at each point of the material and the constant M_S is the saturation magnetization. The magnetic energy is given by the functional $E[\mathbf{n}] = \int d^3r e(\mathbf{r})$, with

$$e(\mathbf{r}) = A \sum_i (\partial_i \mathbf{n})^2 - D \mathbf{z} \cdot (\mathbf{n} \times \partial_z \mathbf{n}) - K (\mathbf{z} \cdot \mathbf{n})^2 - M_S \mathbf{B} \cdot \mathbf{n}. \quad (1)$$

In the above equation the index i runs over $\{x, y, z\}$; A, D , and K denote the exchange stiffness constant, and the DMI and UMA strength constants, respectively; and $\mathbf{B} \mathbf{z}$ is the applied magnetic field. We consider $K < 0$ to have an easy plane perpendicular to \mathbf{z} . The DMI acts only along the z axis, defining the chiral axis (notice that the external field is applied along the chiral axis). The sign of D is reversed if we reverse the direction of the z axis, so that, with no loss of generality, we take $D > 0$. It is convenient to introduce the parameters

$$q_0 = \frac{D}{2A}, \quad \kappa = \frac{4AK}{D^2}, \quad h = \frac{2AM_S}{D^2} B. \quad (2)$$

Notice that q_0 has the dimensions of inverse length while κ and h are dimensionless. We do not include explicitly in the energy the magnetostatic energy, whose effect in an infinite system in which the magnetization depends only on z (as it is in this work) is completely absorbed in the UMA [37].

The dynamics of \mathbf{n} obeys the Landau-Lifschitz-Gilbert (LLG) equation,

$$\partial_t \mathbf{n} = \gamma \mathbf{B}_{\text{eff}} \times \mathbf{n} + \alpha \mathbf{n} \times \partial_t \mathbf{n} + \boldsymbol{\tau}, \quad (3)$$

where α and γ are the Gilbert damping parameter and the gyromagnetic constant, respectively, and $\boldsymbol{\tau}$ denotes some applied nonconservative torque not included in the energy (1). The effective field acting on \mathbf{n} is given by

$$\mathbf{B}_{\text{eff}} = \frac{2A}{M_S} [\nabla^2 \mathbf{n} - 2q_0 \mathbf{z} \times \partial_z \mathbf{n} + q_0^2 \kappa (\mathbf{z} \cdot \mathbf{n}) \mathbf{z} + q_0^2 h \mathbf{z}]. \quad (4)$$

In absence of external torque $\boldsymbol{\tau}$ the equilibrium states are solutions of the static equation $\mathbf{B}_{\text{eff}} = \lambda \mathbf{n}$, where λ is a Lagrange multiplier enforcing the constraint $\mathbf{n}^2 = 1$. For $h \geq h_c$, where $h_c = 1 - \kappa > 1$ is the critical field, the equilibrium state is the homogeneous FFM state, with the magnetization pointing along the z direction: $\mathbf{n} = \mathbf{z}$. For $h < h_c$ the static equation admits solutions which are modulated states with the form of a conical helix propagating along the chiral axis. With the parametrization

$$\mathbf{n} = \sin \theta \cos \varphi \mathbf{x} + \sin \theta \sin \varphi \mathbf{y} + \cos \theta \mathbf{z}, \quad (5)$$

these modulated states are given by [38]

$$\cos \theta_p = \frac{h}{h_c - (p-1)^2}, \quad \varphi_p(z) = pq_0 z, \quad (6)$$

where p is the wave number in units of q_0 . It is convenient to label these states by p , writing θ_p, φ_p , and \mathbf{n}_p . For the sake of brevity, these states will be referred to as the p states, i.e., a p state is a conical state with wave number $q = pq_0$. Since $|\cos \theta_p| \leq 1$, the range of p is limited to

$$1 - \sqrt{h_c - |h|} \leq p \leq 1 + \sqrt{h_c - |h|}. \quad (7)$$

Notice that $h_c > 1$ because we consider easy-plane anisotropy. Hence, for $|h|$ small enough p can be negative. These p states have helicity against the DMI. In a range of h there is also a state with $p = 0$, which is a ferromagnetic state with the magnetization component along the chiral axis given by $n_z = h/(h_c - 1)$. We shall comment on these rather unexpected states in Sec. IV C.

The energy density of the p states is given by

$$e(p) = Aq_0^2 \left[(p-1)^2 - 1 - \frac{h^2}{h_c - (p-1)^2} \right]. \quad (8)$$

The minimum of the energy corresponds to $p = 1$ for all $|h| \leq h_c$, which means that the equilibrium states are those with $p = 1$ (wave number q_0). It is shown in Sec. IV A that for $|h| < h_c$ there exists a range of p around $p = 1$ in which p states are metastable. This implies that these p states are local minima of the energy functional and, therefore, the small perturbations around them are damped as they evolve according to the LLG equation.

The energy density of the p states as a function of p is displayed in Fig. 1 for $h = 0$ and $h = 2 < h_c$, where $h_c = 6$ approximately corresponds to CrNb_3S_6 . The state with minimum energy corresponds always to $p = 1$ (red dots). The

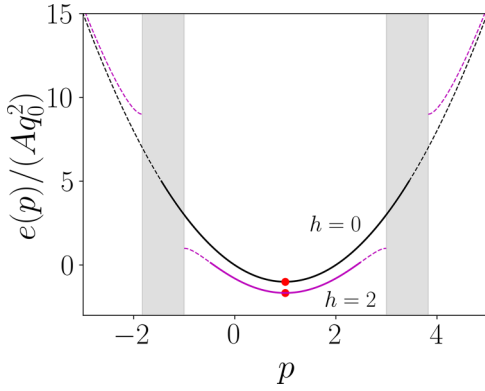


FIG. 1. Energy density for $h = 0$ and $h = 2 < h_c$, as a function of $p = q/q_0$. The minimum value corresponds always to the equilibrium state with $p = 1$. States indicated with continuous lines are stable against localized deformations, while dashed lines indicate unstable states, as shown in Sec. IV A. The gray regions indicate the gap in p values where there are no states satisfying $|\cos \theta_p| \leq 1$.

metastable p states are located in a finite range around $p = 1$ signaled by the continuous lines. Outside this range the p states are unstable (dashed lines). Notice that for $h \neq 0$ there is a gap in p values for which there are no states satisfying $|\cos \theta_p| \leq 1$.

It is remarkable that, in spite of what the form of Fig. 1 may suggest, states with $p \neq 1$ are metastable since the value of p cannot be changed by small perturbations. Indeed, consider a small variation δp of p . A straightforward computation shows that for $\delta p \rightarrow 0$,

$$\mathbf{n}_{p+\delta p} - \mathbf{n}_p \sim 2 \sin \theta_p \sin \left(\frac{\delta p q_0 z}{2} \right) \mathbf{u}(z), \quad (9)$$

where

$$\mathbf{u}(z) = -\sin[(p + \delta p/2)q_0 z] \mathbf{x} + \cos[(p + \delta p/2)q_0 z] \mathbf{y} \quad (10)$$

is a unit vector. This means that a small change of p cannot be considered a small perturbation of \mathbf{n}_p , since $|\mathbf{n}_{p+\delta p} - \mathbf{n}_p|$ is not small for $\delta p q_0 z$ close to π . This may be clearer in a bounded system, of length R , with periodic boundary conditions: Then the minimum δp is $2\pi/q_0 R$ and $0 \leq z \leq R$, so that for this minimum δp we have $\delta p q_0 z = \pi$ if $z = R/2$. Summarizing, the situation is the following: (1) the metastability of a state is related to the behavior of its energy under small perturbations; (2) a change of p , however small, is not a small perturbation of the p state; and (3) it is incorrect to infer from Fig. 1 that the p states are not metastable.

The discussion of the previous paragraph implies that although the energy density of the p states corresponding to p and $p + \delta p$ is close, if the stability ellipses of p and $p + \delta p$ enclose the point $(h, \Gamma = 0)$, then these p states are separated by energy barriers in the whole configuration space of \mathbf{n} for this value of h . How long the lifetime of the metastable p states is depends on these energy barriers. This is a question that cannot be tackled with the methods used in this work. In any case, we expect that the lifetime will increase by decreasing the temperature, a question that deserves further study.

III. STEADY MOTION OF THE CONICAL STATES UNDER THE ACTION OF A POLARIZED CURRENT

In this section we study the response of the p states to a polarized electric current applied along the chiral axis. If the current density is $\mathbf{j} = -j\mathbf{z}$, then the magnetic torque delivered by the current is given by

$$\boldsymbol{\tau} = -jb_j(\partial_z \mathbf{n} - \beta \mathbf{n} \times \partial_z \mathbf{n}), \quad (11)$$

with $b_j = P\mu_B/(|e|M_S)$, where P is the polarization degree of the current, e is the electron charge, and μ_B is the Bohr magneton [39]. The first term is the reactive (adiabatic) torque and the second term the dissipative (nonadiabatic) torque, whose strength is controlled by the nonadiabaticity coefficient β [40].

We start by seeking for steady solutions of the LLG equation (3) which have the form of a state that moves rigidly with constant velocity, v , along the z direction. The general steady solution is characterized by two functions, $\theta(w)$ and $\varphi(w)$, of the variable $w = q_0(z - vt)$. Inserting this *ansatz* in the LLG equations we obtain the steady motion equations, which can be cast to the form

$$\begin{aligned} \theta'' - (\varphi' - 1)^2 \sin \theta \cos \theta + (h_c \cos \theta - h) \sin \theta \\ + \Omega \theta' - \Gamma \sin \theta \varphi' = 0, \end{aligned} \quad (12)$$

$$\sin \theta \varphi'' + 2 \cos \theta \theta' (\varphi' - 1) + \Gamma \theta' + \Omega \sin \theta \varphi' = 0, \quad (13)$$

with the primes standing for derivatives with respect to w and

$$\Omega = \frac{\alpha q_0}{\omega_0} \left(v - \frac{\beta}{\alpha} b_j j \right), \quad (14)$$

$$\Gamma = \frac{q_0}{\omega_0} (v - b_j j), \quad (15)$$

where the quantity $\omega_0 = 2\gamma q_0^2 A/M_S$ has the dimensions of a frequency. Notice that the spin transfer torque, the Gilbert damping, the nonadiabaticity coefficient, and the steady velocity enter the equations of steady motion only through the parameters Ω and Γ .

The solutions of Eqs. (12) and (13) with constant $\theta = \theta_p$ and $\varphi' = p$ correspond to steady moving p states. In this case Eq. (12) is satisfied if

$$\cos \theta_p = \frac{h + p\Gamma}{h_c - (p - 1)^2}. \quad (16)$$

This steady moving p state exists only if $|h + p\Gamma| \leq h_c - (p - 1)^2$. The stability of these solutions is analyzed in Sec. IV A.

To have a solution with constant $\theta = \theta_p$ and $\varphi' = p$ Eq. (13) requires $\Omega = 0$, what provides the relation between the steady velocity and the intensity of the applied current,

$$v = \frac{\beta}{\alpha} b_j j, \quad (17)$$

and thus Γ becomes proportional to the current density,

$$\Gamma = \frac{(\beta - \alpha)q_0}{\alpha\omega_0} b_j j. \quad (18)$$

We see that the steady-state velocity increases linearly with the current density, with a mobility $m = (\beta/\alpha)b_j$ which is independent of the system parameters κ and h . The same

behavior occurs for domain walls [40], for 360° domain walls [41,42], and for the isolated solitons and the chiral soliton lattice of monoaxial chiral helimagnets [43–45]. Therefore this relation between steady velocity and applied current density seems to be a universal feature of the response of one dimensional magnetic modulated states to polarized currents.

Equation (17) implies that $v = 0$ if $\beta = 0$, so that the steady moving solution is actually static if there is no dissipative torque. In this case, after applying the current the system reaches a different equilibrium state, a static p state with cone angle given by equation (16). Notice also that the case $\beta = \alpha$ is special, since then $\Omega = 0$ and $\Gamma = 0$, and therefore Eqs. (12) and (13) are independent of the applied current. This implies that in this case the p state is rigidly dragged by the current, with velocity $v = b_j j$, keeping the cone angle equal to its static value.

IV. STABILITY OF THE MAGNETIC STATES

In this section we analyze the stability of magnetic states against small perturbations. The section is divided into three subsections: One dealing with the stability of the p states, another one devoted to the stability of the FFM state, and the last one in which we discuss the main features of the stability diagram.

A. Stability of the conical states

We analyze here the stability of the generic steady moving p state obtained for given h and Γ . The static p states discussed in Sec. II are the particular cases $\Gamma = 0$ of this general analysis. Here a p state is a steady moving state if $\Gamma \neq 0$ and a static state if $\Gamma = 0$.

Let \mathbf{n}_p be the (unitary) magnetization field of the steady moving p state, with θ_p described by (16) and $\varphi_p = pq_0(z - vt)$, with v given by (17). A small perturbation of \mathbf{n}_p is given by two fields, ξ_1 and ξ_2 , which depend on the three coordinates x, y, z , and on time t , so that, for small-enough ξ_1 and ξ_2 , the perturbed magnetization is given by

$$\mathbf{n} = \sqrt{1 - \xi_1^2 - \xi_2^2} \mathbf{n}_p + \xi_1 \mathbf{e}_1 + \xi_2 \mathbf{e}_2, \quad (19)$$

where $\{\mathbf{e}_1, \mathbf{e}_2, \mathbf{n}_p\}$ form a right-handed orthonormal triad. We take

$$\mathbf{e}_1 = \cos \theta_p \cos \varphi_p \mathbf{x} + \cos \theta_p \sin \varphi_p \mathbf{y} - \sin \theta_p \mathbf{z}, \quad (20)$$

$$\mathbf{e}_2 = -\sin \varphi_p \mathbf{x} + \cos \varphi_p \mathbf{y}. \quad (21)$$

We require that, for fixed t , the fields ξ_1 and ξ_2 be square integrable functions of (x, y, z) , to ensure that the energy of the perturbation is finite.

The perturbed magnetization has to be a solution of the LLG equation. Inserting Eq. (19) into Eq. (3) we obtain the equations for the dynamics of the perturbation $\xi = (\xi_1, \xi_2)^T$. Expanding in powers of ξ_1 and ξ_2 , we have to linear order

$$\partial_t \xi = \frac{\omega_0}{(1 + \alpha^2)q_0^2} \mathcal{D} \xi, \quad (22)$$

where \mathcal{D} is a 2×2 operator matrix whose matrix elements are the linear differential operators,

$$\mathcal{D}_{11} = \alpha(\nabla^2 - a) + [\Delta - (1 + \alpha\beta)b]\partial_z, \quad (23)$$

$$\mathcal{D}_{12} = \nabla^2 - [\alpha\Delta + (\beta - \alpha)b]\partial_z, \quad (24)$$

$$\mathcal{D}_{21} = -\nabla^2 + a + [\alpha\Delta + (\beta - \alpha)b]\partial_z, \quad (25)$$

$$\mathcal{D}_{22} = \alpha\nabla^2 + [\Delta - (1 + \alpha\beta)b]\partial_z, \quad (26)$$

with

$$a = q_0^2 [h_c - (p - 1)^2] \sin^2 \theta_p, \quad (27)$$

$$\Delta = q_0 2(p - 1) \cos \theta_p, \quad b = \frac{q_0 \alpha}{\beta - \alpha} \Gamma, \quad (28)$$

where we assumed $\alpha \neq \beta$. The case $\alpha = \beta$ is special, as we said before, since then $\Gamma = 0$ for any value of the applied current. In this case $b = q_0^2 b_j j / \omega_0$.

Stability requires that the spectrum of \mathcal{D} lies in the complex half-plane with non-negative real part. Since \mathcal{D}_{ij} are linear differential operators with constant coefficients, the spectrum of \mathcal{D} can be readily obtained by Fourier transform. Details on the calculations leading to the stability conditions are given in Appendix A. Here we collect the conclusions. A necessary condition for stability is $a \geq 0$, which gives the following bounds for the p values of stable p states:

$$1 - \sqrt{h_c} \leq p \leq 1 + \sqrt{h_c}. \quad (29)$$

It is shown in Appendix A that, having p within these bounds, the p state is stable only in the region of the (h, Γ) plane enclosed by the ellipse of equation

$$A(p)\Gamma^2 + 2B(p)\Gamma h + C(p)h^2 = D(p), \quad (30)$$

where the functions $A(p)$, $B(p)$, $C(p)$, and $D(p)$ are independent of h and Γ and are given in Appendix A. The stability ellipses of the p states are centered at $(0, 0)$ and have the principal axes rotated with respect to the coordinate axes. The amount of rotation depends on p .

The stability of the static p states discussed in Sec. II is obtained by setting $\Gamma = 0$ in this general approach. Thus, the static p state is stable in the range of h determined by the intersection of its stability ellipse with the $\Gamma = 0$ axis.

Figure 2 displays the stability ellipses for several values of p in the (h, Γ) plane, for $h_c = 6$, which approximately corresponds to CrNb₃S₆. For each p value, the p state is metastable for (h, Γ) inside the corresponding ellipse and unstable outside it.

The region of the (h, Γ) plane in which there exists some stable steady moving p state is bounded by the envelope of the one-parametric family of ellipses (parametrized by p) given by Eq. (30). The envelope can be readily found and it has four branches given by

$$\Gamma = \sigma(h) 2 [1 \pm \sqrt{|h| - (h_c - 1)}], \quad (31)$$

$$\Gamma = -h \pm 2\sqrt{h_c} [\sqrt{h_c(h_c - 1)} - \sqrt{h_c h - h_c}],$$

where $\sigma(h)$ is the sign function: $\sigma(h) = 1$ if $h \geq 0$ and $\sigma(h) = -1$ if $h < 0$. The parametric equations of the envelop are

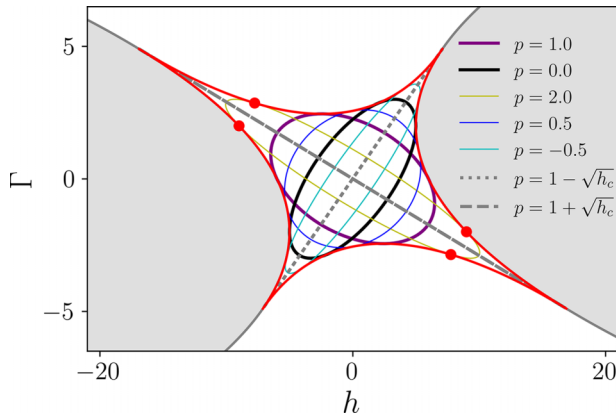


FIG. 2. Stability diagram in the plane (h, Γ) for $h_c = 6$. Steady moving p states are stable inside the region bounded by the red line. The FFM states are only stable within shaded regions, which are unbounded. Red dots correspond to the stability limit of states with $p = 2$ lying in the boundary of the stability diagram, as those shown in Fig. 3.

given in Appendix A, Eqs. (A13)–(A16). We call the region enclosed by this envelope the *stability region of conical states*. No modulated state is stable outside this region.

The four branches of the envelope in the case $h_c = 6$ are shown in red in Fig. 2. Along each branch p changes continuously within its bounds, from $1 - \sqrt{h_c}$ to $1 + \sqrt{h_c}$. Each ellipse, determined by a given value of p , is tangent to the envelope at four points, one for each branch. These four points, which depend on p , define the four pairs of functions shown in Fig. 3. The red points in Figs. 2 and 3 correspond to $p = 2$. The detailed features of the stability diagram will be further discussed in Sec. IV C.

B. Stability of the forced ferromagnetic state

The FFM state is the magnetic texture with a uniform magnetization aligned with the applied field, which in our case points to the direction of the chiral axis z . Hence, the FFM is given by $\mathbf{n} = z$ if $h \geq 0$ and $\mathbf{n} = -z$ if $h < 0$. It is the equilibrium state if $|h| > h_c$. The FFM state is insensitive to an applied current, since the torque (11) vanishes for uniform magnetization. However, it is destabilized by a sufficiently intense current. In this section we discuss the stability diagram of the FFM state in the applied field–applied current plane.

The perturbed FFM state has the form

$$\mathbf{n} = \sqrt{1 - \xi_1^2 - \xi_2^2} \sigma(h) \mathbf{z} + \xi_1 \sigma(h) \mathbf{x} + \xi_2 \mathbf{y}, \quad (32)$$

where $\sigma(h) = 1$ if $h \geq 0$ and $\sigma(h) = -1$ if $h < 0$. The dynamics of the perturbation is obtained by inserting the above expression in the LLG equation (3). Again, the linearized LLG equation is given by a linear differential operator with constant coefficients whose spectrum is obtained by Fourier transform. The stability of the FFM state requires that the spectrum lies in the complex plane with nonpositive real part. The details of the calculations are given in Appendix B. The stability condition leads to the inequality

$$\Gamma^2 - 4\sigma(h)\Gamma + 4(h_c - |h|) \leq 0, \quad (33)$$

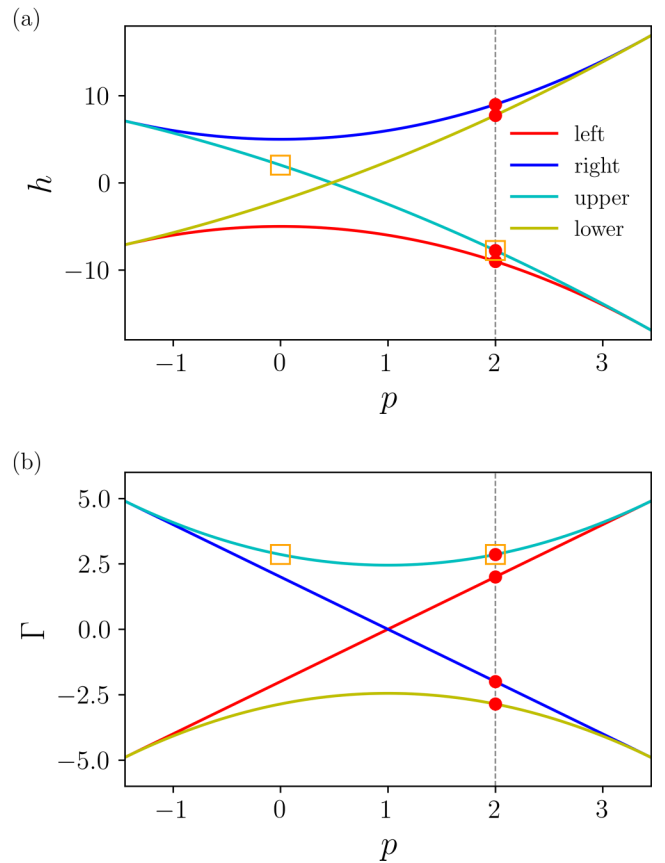


FIG. 3. The values of (a) h and (b) Γ as a function of p along the different branches of the envelope of the stability region defined by Eqs. (31). For a given value of p the four branches (left, right, upper, lower) are presented, corresponding to those shown in Fig. 2. Red dots correspond to those shown in Fig. 2. Square symbols indicate (h, Γ) points for which states with $p = 0$ and $p = 2$ are obtained in Sec. V.

where Γ is related to the current intensity, j , by Eq. (18). The FFM state is stable in the region of the (h, Γ) plane in which the above inequality holds.

Inequality (33) holds if and only if the two roots in Γ of the left-hand side of the inequality are real and Γ is between the two roots. Then $|h| > h_c - 1$ and

$$2(1 - \zeta(h)) \leq \sigma(h)\Gamma \leq 2[1 + \zeta(h)], \quad (34)$$

with $\zeta(h) = \sqrt{1 + |h| - h_c}$. The above inequalities determine the region of stability of the FFM state in the (h, Γ) plane, which is displayed in Fig. 2 for $h_c = 6$.

It is remarkable that the boundary of the stability region of the FFM state coincides exactly with the left and right branches of the boundary of the stability region of conical states. This means that modulated states and the FFM state do not coexist in any region of the (h, Γ) plane. Although in the model domains of FFM and conical states cannot coexist, it is possible to observe domain coexistence in real materials, where dipolar interactions, granularity or disorder effects are present. However, it is always possible to have domains with different p states within the boundary of the stability region.

C. Outstanding features of the stability diagram

There are some characteristics in the stability diagram which have interesting consequences both from a theoretical and applied point of view. Below we enumerate these remarkable features and some of their consequences. Of special relevance is the discussion of point 3 below.

1. Destabilization of p states

At each point (h, Γ) within the stability region of conical states the stable p states are those whose stability ellipse encloses the point. Since all stability ellipses are centered at the origin in the (h, Γ) plane, the only stable p states are those which are metastable at $h = 0$ and $\Gamma = 0$, that is, which are metastable in absence of applied field and current. They are precisely those with p in the range (29). The application of a field and/or a current does not stabilize any other p state, but it destabilizes some of them. As the point (h, Γ) moves away from the origin, it crosses some ellipses, and the corresponding p states become unstable. Outside the stability region of conical states, whose boundary is given by Eqs. (31), no p state is stable.

2. Range of stable p states

One conclusion of the discussion of point 1 above is that at each point (h, Γ) the stable p states have p in a certain range $p_{\min}(h, \Gamma) \leq p \leq p_{\max}(h, \Gamma)$. These two values, $p_{\min}(h, \Gamma)$ and $p_{\max}(h, \Gamma)$, are given by the two real roots of

$$A(p)\Gamma^2 + 2B(p)h\Gamma + C(p)h^2 - D(p) = 0, \quad (35)$$

that lie within the bounds given by Eq. (29). These two values, p_{\min} and p_{\max} , approach each other as (h, Γ) attains the stability boundary of conical states. Therefore, the closest (h, Γ) is to this stability boundary, the narrower the range of p values of stable p states.

3. Manipulating conical states

The discussion of point 1 above suggests a method to switch between metastable conical states with different wave number. For instance, suppose we start at $h = 0$ and $\Gamma = 0$ with some metastable p state, say, with $p \approx 1$. If we apply a field and a polarized current such that (h, Γ) corresponds to a point close to one of the red points of Fig. 2, then the initial p state becomes unstable and it will evolve to one of the p states within the stability range at (h, Γ) . Since this point is close to one of the red points of Fig. 2, where the stability range is narrow, the final p state will have $p \approx 2$. Since this state is metastable also for $h = 0$ and $\Gamma = 0$, it will remain as the field and the current are switched off. Hence, the consequence of this process is to switch the p state from $p \approx 1$ to $p \approx 2$. In Sec. V we will show using numerical simulations that these processes are feasible.

Therefore, a given p state can be selected with high precision by approaching the appropriate point of the stability boundary. The values of h and Γ appropriate to select a conical state with wave number $q \approx pq_0$ are those represented in Fig. 3.

4. Helicity switching

Since for the easy-plane anisotropy considered in this work $h_c > 1$, we have that $1 - \sqrt{h_c} < 0$. This means that there are $p < 0$ within the stability range (29), and the corresponding p states are stable within their stability ellipse. These p states with $p < 0$ are conical states with helicity against the DMI. The metastability of these states opens the possibility of helicity switching in monoaxial chiral helimagnets through the action of a polarized current by means of the process described in point 3 above.

5. Ferromagnetic states

For the same reason $p = 0$ is within the bounds (29). Hence, the p state with $p = 0$ is metastable within its stability ellipse (the black ellipse in Fig. 2). These states are ferromagnetic, with a uniform magnetization which has a component $n_z = \cos\theta_p = h/(h_c - 1)$ along the chiral axis. The magnetization component lying on the plane perpendicular to the chiral axis is undetermined, which means that these ferromagnetic states are highly degenerate. This degeneracy is tantamount to the translational degeneracy of the conical p states. Notice that these ferromagnetic states are different from the FFM state obtained for a sufficiently large magnetic field, in which the magnetization is aligned with the field. Instead, they would be the equilibrium states in absence of DMI, which survive as metastable states when the DMI is present.

6. Supercritical modulated states

The fact that the stability region of the FFM state is convex (see Fig. 2) implies that there are steady moving p states for supercritical applied fields ($|h| > h_c$). This means that if we start with the FFM state with h in an appropriate range, such that $|h| > h_c$, and apply a polarized current of appropriate intensity, then the FFM state will be destabilized and will evolve to attain a steady moving p state: A modulation will be created by the polarized current at a supercritical field. If the current is switched off, then the FFM state will be recovered. One process of this kind is illustrated by micromagnetic simulations in Sec. V.

V. MANIPULATION OF THE CONICAL STATES

The peculiarities of the stability diagram suggest a method to manipulate the conical states described in Sec. IV C, point 3. In this section we illustrate that these ideas are sound by solving the LLG equation with appropriate initial conditions and time-dependent applied field and current by means of micromagnetic simulations.

The micromagnetic numerical simulations are performed using the MuMax3 code [46,47] in which a monoaxial DMI was implemented [43] to model the system given by Eqs. (1) and (11), with material parameters appropriate for CrNb₃S₆ [43]: $A = 1.42$ pJ/m, $D = 369$ μ J/m², $K = -124$ kJ/m³, and $M_S = 129$ kA/m (see Osorio *et al.* [48] for further details). With these parameters the equilibrium pitch of the helical state is $L_0 = 2\pi/q_0 \approx 50$ nm and the critical magnetic field h_c corresponds to $B_c \approx 2300$ mT. The simulations are performed for a one-dimensional system of linear size

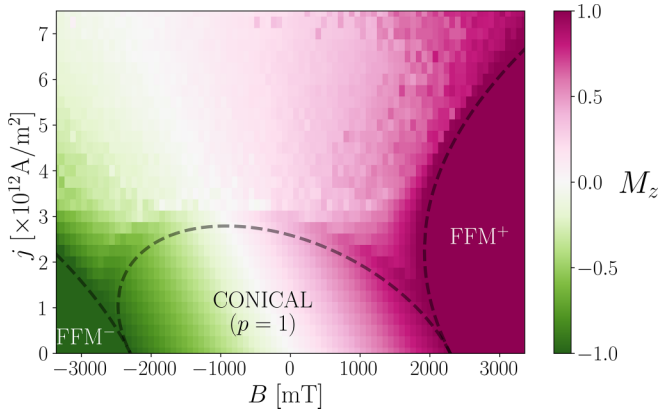


FIG. 4. Stability region for the equilibrium $p = 1$ state ($q = q_0$) for applied magnetic field B and current j , as obtained by numerical simulations. The regions where the FFM states are stable are also shown. The dashed lines correspond to the stability limits.

$R = 500$ nm, with a mesh size $\Delta R = 1$ nm and periodic boundary conditions. We set $\alpha = 0.01$ and $\beta = 0.02$. Notice that in a finite system with periodic boundary condition only a discrete number of 2π rotations can be attained. We denote by Q the winding number (see Ref. [48] for the definition of Q), and $Q_0 = R/L_0 = 10$ is the equilibrium winding number, which corresponds to the p state with $p = 1$. Hence $p = L_0/L = Q/Q_0$ takes only discrete values with step size $1/Q_0 = 1/10$.

Let us start showing the stability diagram corresponding to the equilibrium p state ($p = 1$) obtained from numerical simulations. Given a point (h, Γ) of the stability diagram, the initial state is either the p state with $p = 1$ if $|h + \Gamma| \leq h_c$ (this is the existence condition of the $p = 1$ state) or the FFM state otherwise. A perturbation of small intensity, $M_S/10$, and random orientation is added to the magnetization of the initial state. Then the current is applied for 20 ns. Figure 4 displays the stability region and the corresponding stability ellipse (see Fig. 2). The stability limits of the FFM are also shown in the figure. The stability boundaries are in good agreement with the analysis in Sec. IV B.

In order to show how the system can be manipulated to obtain different targeted p states we use the following protocol. The system is initialized at $(h = 0, \Gamma = 0)$ in a state with a winding number $Q_0 = 10$, which corresponds to the equilibrium state with $p = 1$. A small random perturbation is added to the three components of the magnetization, so that the initial state is actually a perturbed p state. Then a simultaneous square pulse of magnetic field and polarized current with $(h = h_a, \Gamma = \Gamma_a)$ is applied during 20 ns, and afterwards the system is allowed to relax to some metastable state at $(h = 0, \Gamma = 0)$. The evolution of the system can be followed by monitoring the time evolution of the magnetization along the chiral axis, which accounts for the conical distortion, and the winding number $Q \propto p$. A small pulse length is necessary to destabilize the initial state. We expect the final state to depend on the initial perturbation and the shape of the pulse but not on the length of the pulse, since once a new state has been reached it is metastably retained.

Figure 5 shows how different p states can be stabilized following the main diagonals of the ellipses. In Fig. 5(a) results

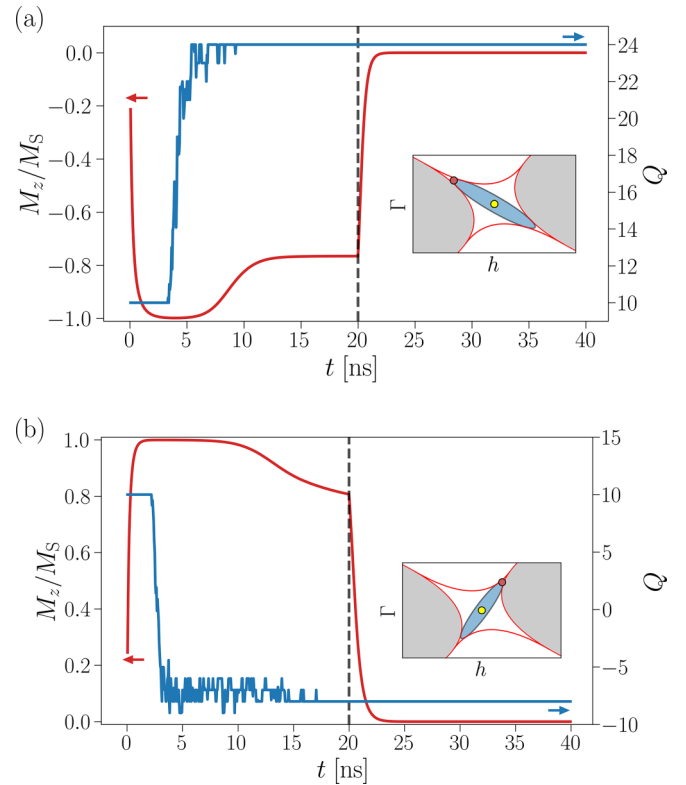


FIG. 5. Evolution of the system when a simultaneous (h_a, Γ_a) square pulse is applied during 20 ns: The red and blue curves represent the net magnetization along z and the winding number, respectively. The dashed black line indicates the moment the pulse is turned off. Initially the system is at $(h = 0, \Gamma = 0)$ (yellow point in the inset) and is characterized by a winding number $Q_0 = 10$. The values of (h_a, Γ_a) (red points in the inset) are in one semiaxis of the shown ellipses corresponding to positive $p = 2$ in (a) and negative $p = -0.5$ in (b).

are presented for $(h_a < 0, \Gamma_a > 0)$, while results with $(h_a > 0, \Gamma_a > 0)$ are shown in Fig. 5(b). In both cases, (h_a, Γ_a) lies outside the stability region of the Q_0 state. In Fig. 5(a) a final state with $Q = 24$ ($p = 2.4$) is obtained, showing that a combined pulse of magnetic field and current can be used to modify the winding number (p state) in the system. Immediately after applying the pulse the winding number stays constant at $Q = 10$ with a conical distortion (signaled by $M_z \neq 0$) that grows rapidly. After that, the winding number changes from $Q = 10$ to $Q = 24$ and the conical distortion adapts to the new winding number. These changes occur roughly within the first 10 ns and after that the winding number remains constant. In (b), the values of $(h_a > 0, \Gamma_a > 0)$ are such that the only stable p states are those with $p < 0$. The process in this case is similar to that in Fig. 5(a), except that not only the winding number changes, their helicity and the conical distortion are also reversed as Q and M_z , respectively, have changed their sign. Therefore, the numerical results show that in this case a helicity switching can be forced with the final-state metastably retained against the DMI favored rotation direction. This shows how the magnetic configuration can be destabilized in favor of new p states by pushing the system outside the ellipse corresponding to the initial state.

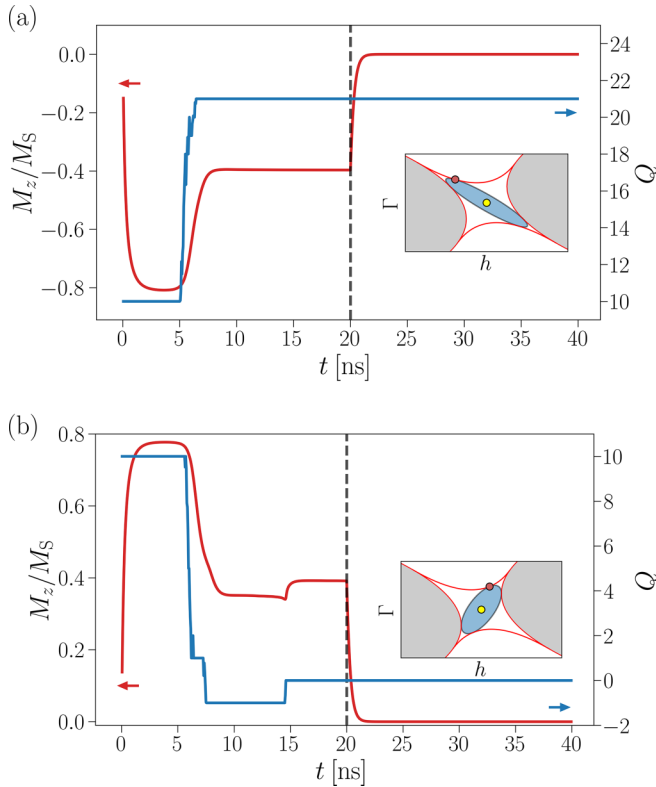


FIG. 6. Evolution of the system when a simultaneous (h_a, Γ_a) square pulse is applied during 20 ns: The red and blue curves represent the net magnetization along z and the winding number, respectively. The dashed black line indicates the moment the pulse is turned off. Initially, the system is at $(h = 0, \Gamma = 0)$ (yellow point in the inset) and is characterized by a winding number $Q_0 = 10$. The values of (h_a, Γ_a) (red points in the inset) are exactly at the point where the ellipses for (a) $p = 2$ and (b) $p = 0$ touch the upper branch of the stability boundary, as shown in the insets.

In order to select a p state with a targeted p value, h_a and Γ_a should be chosen at the stability boundaries, such that $p_{\min} \leq p \leq p_{\max}$ with p_{\min} and p_{\max} very close to each other. Figure 6 presents results using (h_a, Γ_a) close to the stability boundaries and such that (a) $p = 2$ and (b) $p = 0$ are expected (see the square symbols in Fig. 3). Numerical results show that these targeted p states can be readily selected. In Fig. 6(a) $Q = 22$ is obtained, which corresponds to $p = 2.2$, close to the targeted $p = 2$ state. Since we use (h_a, Γ_a) exactly at the point where the ellipse for $p = 2$ touches the stability boundary, the $p = 2$ state is in its stability limit and states very close to $Q = 20$ can be stabilized, in this case $Q = 22$. The evolution of the system for the process shown here is similar to that shown in Fig. 5(a), with a shorter transition timescale. In Fig. 6(b), after fluctuating around $Q = \pm 1$, the final ferromagnetic state with $Q = 0$ is obtained. Note that this state is initially (when $h = h_a$) oriented along a random direction within the cone with $n_z = \cos \theta_p = h_a / (h_c - 1)$, depending on the initial perturbation of the system. The overall evolution in Fig. 6(b) is quite similar to that in Fig. 5(b), but a series of intermediate transitions can be identified. A first transition occurs when the winding number decreases suddenly from $Q = 10$ to $Q = 1$. Then a subsequent transition

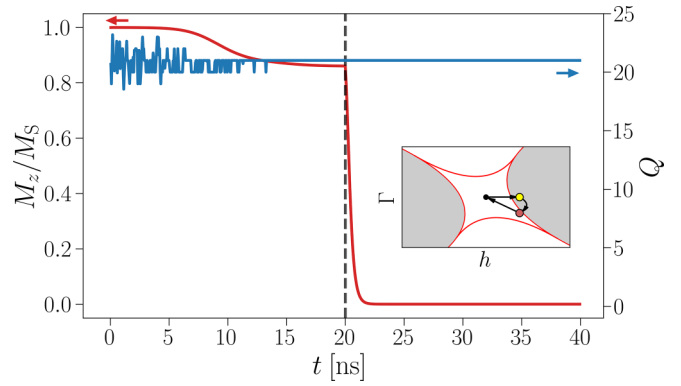


FIG. 7. Switching to a metastable state at zero field using independent field and current pulses. First, a field pulse of intensity $h > h_c$ is used to drive the system to the FFM state (yellow point in the inset). Then, at $t = 0$ a current pulse is applied using a negative Γ value (red dot in the inset) to stabilize the p state. After 20 ns the system is let to relax to a metastable state (the obtained p state) at $(h = 0, \Gamma = 0)$. The dashed black line indicates the moment the pulse is turned off. The red and blue curves represent the net magnetization along z and the winding number, respectively.

is seen in which the system has negative winding number $Q = -1$ (helicity has been reversed). Finally, this modulated state is destroyed and the system reaches the uniform state with $Q = 0$. During all the process the magnetization changes to adapt its value to the corresponding winding number. In particular when the transition to the uniform state takes place (at $t = 15$ ns) a kink in M_z is seen. When $h = 0$ the obtained ferromagnetic state is contained in the easy-plane (xy) defined by the magnetic anisotropy. This ferromagnetic state can be metastably retained, as opposed to the FFM state.

For $\Gamma = 0$, going beyond h_c erases the p state and the FFM state is stabilized. It is important to note that in this case, for a field value $h > h_c$, an applied current can be used to stabilize a p state, as shown in Fig. 7. The system is initialized with $Q_0 = 10$ at $(h = 0, \Gamma = 0)$ and then is set in a FFM state using $(h = h_a > h_c, \Gamma = 0)$. Applying then $\Gamma = \Gamma_a$ inside the stability region, a state with $Q = 21$ is obtained. Immediately after applying the pulse, the winding number abruptly changes from $Q = 0$ and fluctuates around $Q = 21$ to finally remain constant at this value after $t = 15$ ns. It is also seen that the net magnetization along z decreases from $M_z = 1$ (uniform state along the chiral axis) to $M_z \approx 0.85$, indicative of the conical distortion. This state remains when going back to $(h = 0, \Gamma = 0)$. That is, some p states can be created by means of a two-step process: First, the current p state is erased by applying a field higher than h_c and afterwards the FFM state is destabilized by applying an appropriate current. The system evolves to some steady moving stable p state which remains after the field and the current are switched off.

The numerical results shown in this section illustrates how the stability diagram obtained in Sec. IV A can be used to manipulate the conical states.

VI. CONCLUSIONS

Let us summarize the findings reported in this work. Besides the equilibrium state, at low temperature and zero

applied field monoaxial chiral helimagnets have a continuum of helical states differing by the wave number of the modulation [38], which can be written as pq_0 , where q_0 is the wave number of the equilibrium state and p is a dimensionless number. These states are called here the p states. For an infinite system, their energy is a continuum function of p which is minimized by the equilibrium state, corresponding to $p = 1$. These states are local minima of the energy for p in a neighborhood of $p = 1$ [38]. We argued here (Sec. II) that, in spite of what the curve energy *versus* p may suggest (Fig. 1), the p states are metastable in that range.

The application of a magnetic field parallel to the chiral axis has two effects: First, it introduces a conical deformation of the p states and, second, it shrinks the interval of metastability. For applied fields of strength higher than the critical field no p state is stable, and the equilibrium state is the FFM state.

Analogously, the application of a polarized current along the chiral axis has three effects on the p states: First, they reach a steady moving state with a velocity proportional to the intensity of the applied current; second, they suffer a conical deformation similar to that introduced by the application of an external field in the direction of the chiral axis; and, third, some p states are destabilized, and therefore the stability interval shrinks.

The most remarkable fact of the stability diagram of p states in the applied magnetic field–applied current intensity plane (Sec. IV C) is that for each p in the stability range at zero field there are points in the stability diagram at which the interval of stability is very narrow and contains such p . This fact allows us to devise processes to select a given p state. For instance, if we start with some metastable p state at zero current and apply appropriate magnetic field and current, then we end with a steady moving p state with wave number within a narrow interval around the targeted p . This new p state is metastable at zero field and zero current and therefore it would remain as the field and the current are switched off. The feasibility of these processes, which is extremely important from the point of view of applications, is shown by micromagnetic simulations (Sec. V).

Switching between p states opens the possibility of their application in spintronic devices. In particular, there are metastable p states with negative p , and therefore helicity switching is possible in monoaxial chiral helimagnets. It has been argued that controlled switching among magnetic states with opposite helicity might be used for memory applications [36]. Current induced helicity switching has been discussed before in a nonchiral monoaxial helimagnet [49] and in isolated skyrmions in frustrated magnetic systems [50]. In both cases magnetic textures of pure exchange origin were studied, while we report here helicity switching in a monoaxial *chiral* helimagnet, where chirality is due to the presence of DMI.

The p states exist also in cubic chiral magnets [35]. In that case they are characterized not only by the wave number but also by the orientation of the wave vector. The dynamics and stability of the p states of cubic chiral helimagnets under the action of a polarized current have been recently studied by Masell *et al.* [51,52] in the zero applied field case. These authors showed that, under the action of the current, the p

states reach a steady motion state with a velocity proportional to the current density and, at the same time, they suffer a uniform conical deformation with an angle determined by the current. This behavior is the same found here for monoaxial chiral helimagnets. Masell *et al.* found also a critical current which destabilizes the p states. Their analysis of the longitudinal Fourier modes, whose wave vector is parallel to the p state wave vector, gives a destabilizing current which exactly coincides with the result reported here for monoaxial helimagnets, in the particular case $h = 0$, $h_c = 1$, as it must be since by ignoring the transverse fluctuations the cubic chiral helimagnet becomes the monoaxial chiral helimagnet without single-ion anisotropy (UMA). In addition, they found that the p states are destabilized by any current, however small, applied perpendicularly to the wave vector of the p state. This means that the p states tend to propagate along the direction of the applied current. The situation becomes more interesting if there is also an applied field, since in this case the propagation direction of the p state tends to be aligned with the field. Thus, the interplay between the magnitude and relative orientation of the applied field, the applied current, and the p state wave vector promises a complex and rich stability diagram of p states in cubic chiral helimagnets.

The essential question of the lifetime of metastable p states cannot be addressed with the methods of this work. The p states are separated in the magnetic configuration space by energy barriers (they are local minima of the energy functional) and their lifetime depends on the height of such barriers. Thus, it is clear that the lifetime will increase by decreasing the temperature and, therefore, the presence of metastable p states will be more easily detected at low temperature.

The above discussion on lifetimes is related to the experimental signals of the p states. To address these questions it is necessary a careful analysis of the experimental data at low temperature to seek for anomalies attributable to p states. We have already remarked that p states exist also in cubic chiral helimagnets [35]. In these systems the continuum of p states is richer than in monoaxial chiral helimagnets since, besides the wave number, the p states differ also in the orientation of their wave vectors. The low-temperature anomalies reported recently for the cubic chiral helimagnet MnSi [53] may be due to the presence of metastable p states.

ACKNOWLEDGMENTS

Grant No. PID2022-138492NB-I00-XM4 funded by MCIN/AEI/10.13039/501100011033 supported this work. Grants No. OTR02223-SpINS from CSIC/MICIN and No. DGA/M4 from Diputación General de Aragón (Spain) are also acknowledged. This work was also supported by the Grant No. PICT 2017-0906 from the Agencia Nacional de Promoción Científica y Tecnológica, Argentina.

APPENDIX A: STABILITY OF THE CONICAL STATES

A necessary condition for the stability of a p state is that the spectrum of the 2×2 matrix operator \mathcal{D} , whose matrix elements are the linear differential operators given by Eqs. (23)–(26), lies in the complex half-plane with nonpositive real part. The p dependence is hidden in the parameters

a , Δ , and b given by Eqs. (27) and (28). Since the coefficients of those linear operators are constants, the spectrum is easily obtained by Fourier transform.

Denoting the wave vector of the Fourier modes by \mathbf{k} , and setting $k = |\mathbf{k}|$, the spectrum is given by two complex functions of \mathbf{k} , denoted by $\lambda_{\pm}(\mathbf{k})$, given by

$$\lambda_{\pm}(\mathbf{k}) = -\frac{\alpha}{2}(2k^2 + a) + i[\Delta - (1 + \alpha\beta)b]k_z \pm \sqrt{a_r + i a_i}, \quad (\text{A1})$$

where

$$a_r = \frac{\alpha^2 a^2}{4} - k^2(k^2 + a) + [\alpha\Delta + (\beta - \alpha)b]^2 k_z^2, \quad (\text{A2})$$

$$a_i = -[\alpha\Delta + (\beta - \alpha)b](2k^2 + a)k_z. \quad (\text{A3})$$

We only need the real parts, which are given by

$$\text{Re } \lambda_{\pm}(\mathbf{k}) = -\frac{\alpha}{2}(2k^2 + a) \pm \sqrt{\frac{\sqrt{a_r^2 + a_i^2} + a_r}{2}}, \quad (\text{A4})$$

Since $\text{Re} \lambda_+(\mathbf{k}) \geq \text{Re} \lambda_-(\mathbf{k})$, stability requires $\text{Re} \lambda_+(\mathbf{k}) \leq 0$, which, with simple algebraic manipulation, can be shown to be equivalent to

$$[\alpha\Delta + (\beta - \alpha)b]^2 k_z^2 \leq \alpha^2 k^2 (k^2 + a). \quad (\text{A5})$$

Since the left-hand side of this inequality is non-negative, and since it must hold for any k , and in particular for $k \rightarrow 0$, we get $a \geq 0$. This relation sets the bounds for the p values of stable p states given by the inequalities (29).

Since $a \geq 0$, the right-hand side of (A5) increases with $k_x^2 + k_y^2$, and therefore the inequality is satisfied if and only if it is satisfied for $k_x^2 + k_y^2 = 0$. Thus we set $k^2 = k_z^2$, and then we have

$$k_z^2 [k_z^2 + a - (\Delta + q_0 \Gamma)^2] \geq 0. \quad (\text{A6})$$

Noticing that with $a \geq 0$ inequality (A5) holds for all \mathbf{k} if and only if it holds for $\mathbf{k} = k_z \mathbf{z}$, the stability condition reduces to $(\Delta + q_0 \Gamma)^2 \leq a$. To arrive to this inequality Eq. (18) was used. Substituting the expressions for a , Δ and $\cos \theta_p$ in this inequality we get the following expression for the stability condition:

$$A(p)\Gamma^2 + 2B(p)\Gamma h + C(p)h^2 \leq D(p), \quad (\text{A7})$$

where

$$A(p) = 2(p-1)^3 + 3(h_c + 1)(p-1)^2 + 6h_c(p-1) + h_c(h_c + 1), \quad (\text{A8})$$

$$B(p) = (p-1)^3 + 3(p-1)^2 + 3h_c(p-1) + h_c, \quad (\text{A9})$$

$$C(p) = h_c + 3(p-1)^2, \quad (\text{A10})$$

$$D(p) = [h_c - (p-1)^2]^3. \quad (\text{A11})$$

Notice that $D(p) \geq 0$ for p satisfying the bounds (29). The inequality (A7) determines a region in the (h, Γ) plane limited by a conic section. The discriminant of the left-hand side of (A7) is

$$B(p)^2 - A(p)C(p) = -D(p) \leq 0. \quad (\text{A12})$$

Therefore, the conic section is actually an ellipse centered at $(0, 0)$ with the principal axes rotated with respect to the coordinate axes. The amount of rotation depends on p . The steady moving p state is stable within the region of the (h, Γ) plane enclosed by the corresponding ellipse. The stability of the static p states discussed in Sec. II is obtained as a particular case of this general approach, setting $\Gamma = 0$. The static p state is thus stable in the range of h determined by the intersection of its stability ellipse with the $\Gamma = 0$ axis.

The region of the (h, Γ) plane in which there exists some stable steady moving p state is bounded by the envelope of the one-parametric family of ellipses given by Eq. (30). The envelope can be readily found and it has four branches determined by the parametric equations

$$\begin{aligned} h &= -[(p-1)^2 + 2(p-1) + h_c] \\ \Gamma &= 2(p-1), \end{aligned} \quad (\text{A13})$$

$$\begin{aligned} h &= (p-1)^2 + 2(p-1) + h_c \\ \Gamma &= -2(p-1), \end{aligned} \quad (\text{A14})$$

$$\begin{aligned} h &= -[(p-1)^2 + 2h_c(p-1) + h_c]/\sqrt{h_c} \\ \Gamma &= [(p-1)^2 + h_c]/\sqrt{h_c} \end{aligned} \quad (\text{A15})$$

$$\begin{aligned} h &= [(p-1)^2 + 2h_c(p-1) + h_c]/\sqrt{h_c} \\ \Gamma &= -[(p-1)^2 + h_c]/\sqrt{h_c}, \end{aligned} \quad (\text{A16})$$

with p is in the range given by Eq. (29).

The parameter p can be eliminated in each of these four pairs of equations and then the equations of the envelope in the form (31) are obtained. This envelope bounds the region of the (h, Γ) plane where some (steady moving) p state is stable, which in Sec. IV A is called the *stability region of conical states*.

APPENDIX B: STABILITY OF THE FFM

To linear order, the dynamics of perturbations, ξ , of the FFM state obey Eq. (22), in this case with

$$\mathcal{D}_{11} = \alpha(\nabla^2 - a) - [2q_0 + (1 + \alpha\beta)b]\partial_z, \quad (\text{B1})$$

$$\mathcal{D}_{12} = \nabla^2 - a + [\alpha 2q_0 - (\beta - \alpha)b]\partial_z, \quad (\text{B2})$$

$$\mathcal{D}_{21} = -\nabla^2 + a - [\alpha 2q_0 - (\beta - \alpha)b]\partial_z, \quad (\text{B3})$$

$$\mathcal{D}_{22} = \alpha(\nabla^2 - a) - [2q_0 + (1 + \alpha\beta)b]\partial_z, \quad (\text{B4})$$

where now

$$a = q_0^2(|h| + \kappa), \quad b = \sigma(h) \frac{q_0^2 b_j j}{\omega_0} = q_0 \frac{\alpha}{\beta - \alpha} \sigma(h) \Gamma, \quad (\text{B5})$$

with $\sigma(h) = 1$ if $h \geq 0$ and $\sigma(h) = -1$ if $h < 0$.

If the FFM is stable, then the spectrum of \mathcal{D} lies on the complex half-plane with nonpositive real part. Again, the spectrum of \mathcal{D} is easily obtained by Fourier transform. If, as before, \mathbf{k} is the wave vector of the Fourier mode, the spectrum is given by the complex functions $\lambda_{\pm}(\mathbf{k})$, whose real parts are

$$\text{Re } \lambda_{\pm}(\mathbf{k}) = -\alpha(k^2 + a) \pm [\alpha 2q_0 - (\beta - \alpha)b]k_z. \quad (\text{B6})$$

Now $\text{Re } \lambda_{\pm}(\mathbf{k}) \leq 0$ if and only if

$$\alpha k_z^2 \pm [\alpha 2q_0 - (\beta - \alpha)b]k_z + \alpha a \geq 0, \quad (\text{B7})$$

for all real k_z . This means that the two roots in k_z of the left-hand side of the above inequality must be either complex or equal, that is, the discriminant of the quadratic polynomial in k_z given by the left-hand side of the above inequality must be nonpositive:

$$[\alpha 2q_0 - (\beta - \alpha)b]^2 - 4\alpha^2 a \leq 0. \quad (\text{B8})$$

Inserting the values of a and b given by Eq. (B5) and defining Γ by Eq. (18) we obtain

$$\Gamma^2 - 4\sigma(h)\Gamma + 4(h_c - |h|) \leq 0. \quad (\text{B9})$$

To have a nonempty solution of this inequality the two roots in Γ of its left-hand side must be real, and then the inequality holds for Γ being between the two roots. Then we get the condition $|h| > h_c - 1$ and if this holds, then the two roots are given by

$$\Gamma_{\pm} = \sigma(h)2[1 \pm \zeta(h)], \quad (\text{B10})$$

with $\zeta(h) = \sqrt{1 + |h| - h_c}$. In this way we obtain that the stability region of the FFM state in the (h, Γ) plane is determined by the inequalities (34). It is remarkable that the boundary of the stability region of the FFM state coincides exactly with two of the branches of the boundary of the stability region of conical states. As emphasized at the end of Sec. IV B, this means that conical states never coexist with the FFM state.

-
- [1] L. Berger, Exchange interaction between ferromagnetic domain wall and electric current in very thin metallic films, *J. Appl. Phys.* **55**, 1954 (1984).
- [2] P. Freitas and L. Berger, Observation of s - d exchange force between domain walls and electric current in very thin permalloy films, *J. Appl. Phys.* **57**, 1266 (1985).
- [3] C. Chappert, A. Fert, and F. N. Van Dau, The emergence of spin electronics in data storage, *Nat. Mater.* **6**, 813 (2007).
- [4] S. S. Parkin, M. Hayashi, and L. Thomas, Magnetic domain-wall racetrack memory, *Science* **320**, 190 (2008).
- [5] N. Nagaosa and Y. Tokura, Topological properties and dynamics of magnetic skyrmions, *Nat. Nanotechnol.* **8**, 899 (2013).
- [6] C. Back, V. Cros, H. Ebert, K. Everschor-Sitte, A. Fert, M. Garst, T. Ma, S. Mankovsky, T. Monchesky, M. Mostovoy *et al.*, The 2020 skyrmionics roadmap, *J. Phys. D* **53**, 363001 (2020).
- [7] S. Mühlbauer, B. Binz, F. Jonietz, C. Pfleiderer, A. Rosch, A. Neubauer, R. Georgii, and P. Böni, Skyrmion lattice in a chiral magnet, *Science* **323**, 915 (2009).
- [8] X. Yu, Y. Onose, N. Kanazawa, J. Park, J. Han, Y. Matsui, N. Nagaosa, and Y. Tokura, Real-space observation of a two-dimensional skyrmion crystal, *Nature (London)* **465**, 901 (2010).
- [9] X. Yu, N. Kanazawa, Y. Onose, K. Kimoto, W. Zhang, S. Ishiwata, Y. Matsui, and Y. Tokura, Near room-temperature formation of a skyrmion crystal in thin-films of the helimagnet fege, *Nat. Mater.* **10**, 106 (2011).
- [10] T. Moriya and T. Miyadai, Evidence for the helical spin structure due to antisymmetric exchange interaction in $\text{Cr}_{1/3}\text{NbS}_2$, *Solid State Commun.* **42**, 209 (1982).
- [11] Y. Kousaka, T. Ogura, J. Zhang, P. Miao, S. Lee, S. Torii, T. Kamiyama, J. Campo, K. Inoue, and J. Akimitsu, Long periodic helimagnetic ordering in CrM_3S_6 ($M = \text{Nb}$ and Ta), *J. Phys.: Conf. Ser.* **746**, 012061 (2016).
- [12] B. Roessli, J. Schefer, G. A. Petrakovskii, B. Ouladdiaf, M. Boehm, U. Staub, A. Vorotinov, and L. Bezmaternikh, Formation of a Magnetic Soliton Lattice in Copper Metaborate, *Phys. Rev. Lett.* **86**, 1885 (2001).
- [13] K. Adachi, N. Achiwa, and M. Mekata, Helical magnetic structure in CsCuCl_3 , *J. Phys. Soc. Jpn.* **49**, 545 (1980).
- [14] S. Ohara, S. Fukuta, K. Ohta, H. Kono, T. Yamashita, Y. Matsumoto, and J. Yamaura, Study of chiral structure and magnetism in heavy-fermion $\text{Yb}(\text{Ni}_{1-x}\text{Cu}_x)_3\text{Al}_9$, *JPS Conf. Proc.* **3**, 017016 (2014).
- [15] T. Matsumura, Y. Kita, K. Kubo, Y. Yoshikawa, S. Michimura, T. Inami, Y. Kousaka, K. Inoue, and S. Ohara, Chiral soliton lattice formation in monoaxial helimagnet $\text{Yb}(\text{Ni}_{1-x}\text{Cu}_x)_3\text{Al}_9$, *J. Phys. Soc. Jpn.* **86**, 124702 (2017).
- [16] A. Zheludev, S. Maslov, G. Shirane, Y. Sasago, N. Koide, and K. Uchinokura, Field-Induced Commensurate-Incommensurate Phase Transition in a Dzyaloshinskii-Moriya Spiral Antiferromagnet, *Phys. Rev. Lett.* **78**, 4857 (1997).
- [17] S. K. Karna, F. N. Womack, R. Chapai, D. P. Young, M. Marshall, W. Xie, D. Graf, Y. Wu, H. Cao, L. DeBeer-Schmitt, P. W. Adams, R. Jin, and J. F. DiTusa, Consequences of magnetic ordering in chiral $\text{Mn}_{1/3}\text{NbS}_2$, *Phys. Rev. B* **100**, 184413 (2019).
- [18] S. K. Karna, M. Marshall, W. Xie, L. DeBeer-Schmitt, D. P. Young, I. Vekhter, W. A. Shelton, A. Kovács, M. Charilaou, and J. F. DiTusa, Annihilation and control of chiral domain walls with magnetic fields, *Nano Lett.* **21**, 1205 (2021).
- [19] I. Dzyaloshinskii, Theory of helicoidal structures in antiferromagnets. I. Nonmetals, *Sov. Phys. JETP* **19**, 960 (1964).
- [20] Y. Izyumov, Modulated, or long-periodic, magnetic structures of crystals, *Sov. Phys. Usp.* **27**, 845 (1984).
- [21] J. Kishine, K. Inoue, and Y. Yoshida, Synthesis, structure and magnetic properties of chiral molecule-based magnets, *Prog. Theor. Phys. Suppl.* **159**, 82 (2005).
- [22] Y. Togawa, T. Koyama, K. Takayanagi, S. Mori, Y. Kousaka, J. Akimitsu, S. Nishihara, K. Inoue, A. S. Ovchinnikov, and J. Kishine, Chiral Magnetic Soliton Lattice on a Chiral Helimagnet, *Phys. Rev. Lett.* **108**, 107202 (2012).
- [23] T. Miyadai, K. Kikuchi, H. Kondo, S. Sakka, M. Arai, and Y. Ishikawa, Magnetic properties of $\text{Cr}_{1/3}\text{NbS}_2$, *J. Phys. Soc. Jpn.* **52**, 1394 (1983).
- [24] N. J. Ghimire, M. A. McGuire, D. S. Parker, B. Sipos, S. Tang, J.-Q. Yan, B. C. Sales, and D. Mandrus, Magnetic phase transition in single crystals of the chiral helimagnet $\text{Cr}_{1/3}\text{NbS}_2$, *Phys. Rev. B* **87**, 104403 (2013).
- [25] B. Chapman, A. Bornstein, N. Ghimire, D. Mandrus, and M. Lee, Spin structure of the anisotropic helimagnet $\text{Cr}_{1/3}\text{NbS}_2$ in a magnetic field, *Appl. Phys. Lett.* **105**, 072405 (2014).
- [26] V. Laliena, J. Campo, J. I. Kishine, A. S. Ovchinnikov, Y. Togawa, Y. Kousaka, and K. Inoue, Incommensurate-

- commensurate transitions in the mono-axial chiral helimagnet driven by the magnetic field, *Phys. Rev. B* **93**, 134424 (2016).
- [27] V. Laliena, J. Campo, and Y. Kousaka, Nucleation, instability, and discontinuous phase transitions in the phase diagram of the monoaxial helimagnet with oblique fields, *Phys. Rev. B* **95**, 224410 (2017).
- [28] P. de Gennes, in *Fluctuations, Instabilities, and Phase Transitions*, edited by T. Riste, NATO ASI Ser. B Vol. 2 (Plenum, New York, 1975).
- [29] V. Laliena, J. Campo, and Y. Kousaka, Understanding the H - T phase diagram of the monoaxial helimagnet, *Phys. Rev. B* **94**, 094439 (2016).
- [30] K. Tsuruta, M. Mito, H. Deguchi, J. Kishine, Y. Kousaka, J. Akimitsu, and K. Inoue, Phase diagram of the chiral magnet $\text{Cr}_{1/3}\text{NbS}_2$ in a magnetic field, *Phys. Rev. B* **93**, 104402 (2016).
- [31] J.-i. Yonemura, Y. Shimamoto, T. Kida, D. Yoshizawa, Y. Kousaka, S. Nishihara, F. J. T. Goncalves, J. Akimitsu, K. Inoue, M. Hagiwara, and Y. Togawa, Magnetic solitons and magnetic phase diagram of the hexagonal chiral crystal CrNb_3S_6 in oblique magnetic fields, *Phys. Rev. B* **96**, 184423 (2017).
- [32] E. M. Clements, R. Das, L. Li, P. J. Lampen-Kelley, M.-H. Phan, V. Keppens, D. Mandrus, and H. Srikanth, Critical behavior and macroscopic phase diagram of the monoaxial chiral helimagnet $\text{Cr}_{1/3}\text{NbS}_2$, *Sci. Rep.* **7**, 6545 (2017).
- [33] E. M. Clements, R. Das, M.-H. Phan, L. Li, V. Keppens, D. Mandrus, M. Osofsky, and H. Srikanth, Magnetic field dependence of nonlinear magnetic response and tricritical point in the monoaxial chiral helimagnet $\text{Cr}_{1/3}\text{NbS}_2$, *Phys. Rev. B* **97**, 214438 (2018).
- [34] V. Laliena, Y. Kato, G. Albalade, and J. Campo, Thermal fluctuations in the conical state of monoaxial helimagnets, *Phys. Rev. B* **98**, 144445 (2018).
- [35] V. Laliena and J. Campo, Stability of skyrmion textures and the role of thermal fluctuations in cubic helimagnets: A new intermediate phase at low temperature, *Phys. Rev. B* **96**, 134420 (2017).
- [36] N. Jiang, Y. Nii, H. Arisawa, E. Saitoh, and Y. Onose, Electric current control of spin helicity in an itinerant helimagnet, *Nat. Commun.* **11**, 1601 (2020).
- [37] A. Hubert and R. Schäfer, *Magnetic Domains* (Springer-Verlag, Berlin, 2008).
- [38] V. Laliena, G. Albalade, and J. Campo, Stability of the skyrmion lattice near the critical temperature in cubic helimagnets, *Phys. Rev. B* **98**, 224407 (2018).
- [39] S. Zhang and Z. Li, Roles of Nonequilibrium Conduction Electrons on the Magnetization Dynamics of Ferromagnets, *Phys. Rev. Lett.* **93**, 127204 (2004).
- [40] A. Thiaville, Y. Nakatani, J. Miltat, and Y. Suzuki, Micromagnetic understanding of current-driven domain wall motion in patterned nanowires, *Europhys. Lett.* **69**, 990 (2005).
- [41] M. D. Mascaró and C. A. Ross, ac and dc current-induced motion of a 360° domain wall, *Phys. Rev. B* **82**, 214411 (2010).
- [42] C. Jin, S. Zhang, Q. Zhu, X. Liu, S. Chen, C. Song, J. Wang, and Q. Liu, Current-induced 360° domain wall motion with Dzyaloshinskii-Moriya interaction, *J. Phys. D: Appl. Phys.* **49**, 175005 (2016).
- [43] V. Laliena, S. Bustingorry, and J. Campo, Dynamics of chiral solitons driven by polarized currents in monoaxial helimagnets, *Sci. Rep.* **10**, 20430 (2020).
- [44] S. A. Osorio, A. Athanopoulos, V. Laliena, J. Campo, and S. Bustingorry, Response of the chiral soliton lattice to spin-polarized currents, *Phys. Rev. B* **106**, 094412 (2022).
- [45] J.-i. Kishine, A. S. Ovchinnikov, and I. V. Proskurin, Sliding conductivity of a magnetic kink crystal in a chiral helimagnet, *Phys. Rev. B* **82**, 064407 (2010).
- [46] A. Vansteenkiste, J. Leliaert, M. Dvornik, M. Helsen, F. Garcia-Sanchez, and B. V. Waeyenberge, The design and verification of MuMax³, *AIP Adv.* **4**, 107133 (2014).
- [47] J. Leliaert, M. Dvornik, J. Mulders, J. De Clercq, M. V. Milošević, and B. Van Waeyenberge, Fast micromagnetic simulations on GPU-recent advances made with MuMax³, *J. Phys. D: Appl. Phys.* **51**, 123002 (2018).
- [48] S. A. Osorio, V. Laliena, J. Campo, and S. Bustingorry, Creation of single chiral soliton states in monoaxial helimagnets, *Appl. Phys. Lett.* **119**, 222405 (2021).
- [49] J.-i. Ohe and Y. Onose, Chirality control of the spin structure in monoaxial helimagnets by charge current, *Appl. Phys. Lett.* **118**, 042407 (2021).
- [50] X. Zhang, J. Xia, O. A. Tretiakov, H. T. Diep, G. Zhao, J. Yang, Y. Zhou, M. Ezawa, and X. Liu, Current-induced helicity switching of frustrated skyrmions on a square-grid obstacle pattern, *J. Magn. Soc. Jpn.* **47**, 20 (2023).
- [51] J. Masell, X. Yu, N. Kanazawa, Y. Tokura, and N. Nagaosa, Combing the helical phase of chiral magnets with electric currents, *Phys. Rev. B* **102**, 180402(R) (2020).
- [52] J. Masell, X. Yu, N. Kanazawa, Y. Tokura, and N. Nagaosa, Manipulating the helical phase of chiral magnets with electric currents, [arXiv:2007.03414v1](https://arxiv.org/abs/2007.03414).
- [53] M. Ohkuma, M. Mito, M. Pardo, Y. Kousaka, S. Iwasaki, K. Ohishi, J. Akimitsu, K. Inoue, V. Laliena, and J. Campo, New magnetic intermediate state, “B-phase”, in the cubic chiral magnet MnSi, *APL Mater.* **10**, 041104 (2022).